Angular Misalignment Measurements for an Off-Plane Reflection Grating Module

G. Grell[1], R. Smith[2], C. DeRoo[2], R. Allured[2], E. Hertz[2], J. Kolodziejczak[3], J. Gaskin[3], S. O'Dell[3], R. McEntaffer[4], D. Miles[4]

ABSTRACT

We present an analysis of an alignment technique used for an off-plane reflection grating system that, if proven to be feasible, would ideally be utilized for future astronomical x-ray spectrometers. The use of reflection gratings allows for the production of both high throughput and spectral resolution. As such, they are a candidate grating technology for future soft X-ray spectroscopy missions. To be viable for these missions, however, a low-cost optical technique for co-aligning multiple gratings into a module for use in a spectrograph must be demonstrated. The off-plane grating module was built to contain fifteen gratings with proper relative alignment to one another for a converging X-ray beam. The module was coupled with a silicon pore optic mirror to produce a spectrum of reflected and diffracted light onto a CCD camera at the focal plane. The alignment performance of the module's grating system was assessed both before and after a series of vibrational and thermal tests were conducted at the NASA Marshall Space Flight Center. Data reduction was done in order to identify the number and position of photon events from the diffraction spots for each grating, and raytracing analysis was conducted in order to calculate the induced grating-to-grating angular misalignments. Finally, these measurements were compared to theoretical alignment tolerances derived using analytical techniques. The grating system yielded misalignments within a factor of 2-3 of the analytical tolerances, which is very encouraging for a first attempt. Further refinement and troubleshooting is required to see whether or not this alignment technique can be used in the future.

[1]Harvard University, Astronomy 98

[2]Smithsonian Astrophysical Observatory

[3]NASA Marshall Space Flight Center

[4]Pennsylvania State University

1. Introduction

X-ray spectroscopy is a powerful tool for observing some of the most energetic events in the Universe. The current generation of high-resolution X-ray spectrographs have enabled effective investigations of stellar evolution, black hole feedback, and galaxy structure. One of the most successful of these instruments has been NASA's *Chandra X-ray Observatory*, which has played a pivotal role in obtaining high-resolution spectra and feedback from a range of celestial phenomena, including supermassive black holes, neutron stars, stellar coronae, and shocked stellar winds (Tananbaum et al. 2014). Chandra's sub-arcsecond angular resolution, which enables it's high-resolution imaging capability, is the key to these discoveries (Weisskopf et al. 2002). Another observatory of equal stature has been the *XMM-Newton*, which is equipped with a reflection grating system that allows for a superior effective collecting area for spectroscopy (Lumb et al. 2012).

The problem with current X-ray spectrometers is that they fall short of their potential in terms of both resolution and efficiency. The effective areas of current missions are typically less than 10% of X-ray imaging missions, and current resolutions are $R = \lambda/\Delta\lambda < 1000$ (Smith et al. 2016). As a result, these missions cannot effectively survey cosmological phenomena, like hot low density gas, beyond the edges of galaxies and clusters. These limitations are holding back the field as a whole, as most of the baryons in the Universe are typically found in these outskirt regions (Simionescu et al. 2011). Goals of future X-ray missions include both enabling the ability to reach these regions and providing more efficient feedback.

The use of off-plane reflection gratings, which enables the production of high throughput and spectral resolution at low energy ranges, is a potential solution (McEntaffer et al. 2013). Using these gratings, future x-ray spectrometers would be able to provide data necessary to identify astrophysical models for galaxy and large-scale formation, as well as easily detect absorption line features (Smith et al. 2016). Potential long-term goals for these spectrometers include observing the outcome of structure formation beyond the edges of galaxy clusters, observing the evolution of stellar coronae, and observing feedback from supermassive black holes (Smith et al. 2016).

The goal of this project was to demonstrate the feasibility of fabricating off-plane grating modules in a flight-like mount. This involved aligning and bonding gratings into a housing module, assembling and correctly positioning a setup composed of the OPG module, a silicon pore optic module, and CCD camera in a vacuum chamber, testing the grating-to-grating alignment prior to and after implementing environmental tests, and using raytracing sensitivity analysis to derive the degree of angular misalignments that occurred between gratings by analyzing diffraction spot images taken by the CCD. Section 2 of this paper

describes the off-plane grating geometry. Section 3 describes the module design and grating alignment procedure, as well as an overview of the alignment performance tests that took place at the Marshall Space Flight Center. Section 4 describes the data reduction and counting methods used to measure photon events, and the photon count results. Section 5 describes the raytracing sensitivity analysis and shows the calculations of the grating-to-grating angular misalignments. Section 6 is a discussion of the results and future directions.

2. Off-Plane Grating Geometry

In order to achieve the optimal level of spectral resolution and collecting area, an off-plane grating system must meet a series of geometric requirements (DeRoo et al. 2016). For high spectral resolving power, each grating requires blazed radial groove profiles that are oriented such that they are nearly parallel to direction of the incoming light. The grooves are radial to decrease the spacing between adjacent grooves towards the focus, in order to match the telescope beam convergence (McEntaffer et al. 2013, Marlowe et al. 2015). In addition, these grooves are blazed to a specific angle to diffract light to one side of zero order (reflection), thus optimizing efficiency. This grating geometry creates diffraction arcs at the focal plane, with dispersion determined by the grating equation shown in **Figure 1**. This result is what distinguishes OPGs from other grating systems, as the *off-plane* in the term refers to the fact that the produced dispersion direction is outside of the incidence plane in the shape of a cone.

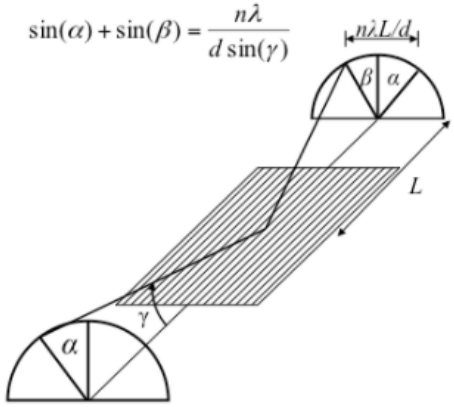

Fig. 1.—: Off-plane grating geometry. The diffraction arcs at the focal plane with dispersion are determined by the displayed grating equation. γ: the half-cone polar angle between the incident light beam and the groove axis, d: the line spacing of the grooves, n: the diffraction order, α: the azimuthal angle between the reflected spot and the grating normal, β: the azimuthal angle between the diffracted spot and grating normal. (DeRoo et al. 2016, Marlowe et al. 2015)

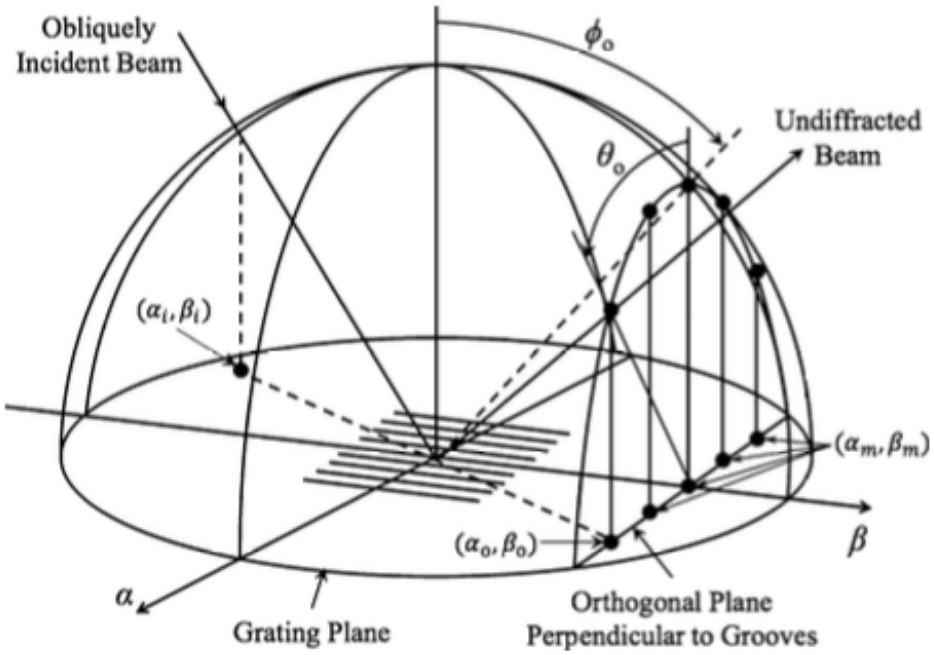

Fig. 2.—: Three-dimensional view of the diffraction arc created from an off-plane reflection grating. α_0 and β_0 represent the coordinates of the zero order spot, α_i and β_i represent the coordinates of the incident beam spot, and α_m and β_m represent the coordinates of each diffraction order m (Allured and McEntaffer 2013).

The next step is aligning each individual grating to one another. The gratings must be aligned such that the diffracted spectra overlap at the focal plane (Allured & McEntaffer 2013). This step, which will be described in further detail in **Section 3.2**, is essential for the overall system, as failure to completely align the diffraction arcs results in the loss of spectral resolution. Additionally, the gratings must be stacked together into an array, in order to maximize the effective collecting area. An illustration of these requirements is shown in **Figure 3**, which has the optical axis pointing out of the page.

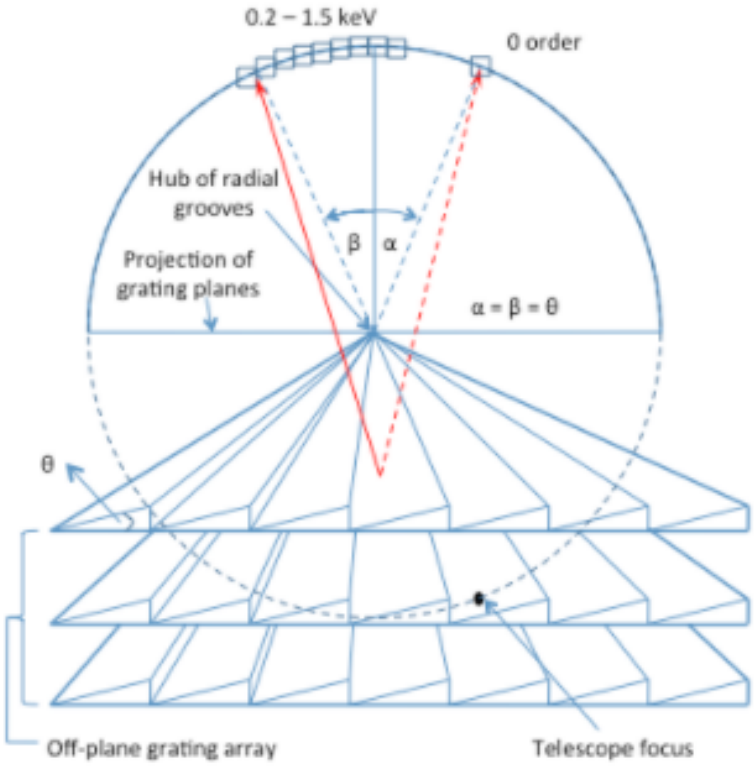

Fig. 3.—: Three co-aligned gratings projected onto the focal plane along with their diffraction arc. Each grating's diffraction arc overlaps with the others at the focal plane (Allured & McEntaffer 2013).

The utilization of OPGs, along with custom groove profiles, in this geometric setup will allow for the target resolution and collecting area. However, the main drawback of this technique is the very tight amount of alignment tolerance that is allowed. Alignment tolerances must be taken into consideration because excessive angular misalignment will result in the loss of both spectral resolution and effective area.

Allured & McEntaffer 2013 analytically quantified these tolerances for a general off-plane system, as they calculated the maximum misalignment such that a shift in the x-coordinate (Δx) of a diffracted spot would be less than or equal to 40 micrometers. This calculation was done in all six degrees of freedom (defined in **Figure 4**): linear motion in the dispersion direction $\hat{x}$, linear motion in the cross-dispersion direction $\hat{y}$, $\hat{z}$, pitch (rotations about $\hat{x}$), yaw (rotations about $\hat{y}$), and roll (rotations about $\hat{z}$). The calculated tolerance for each degree is shown in **Table 1**.

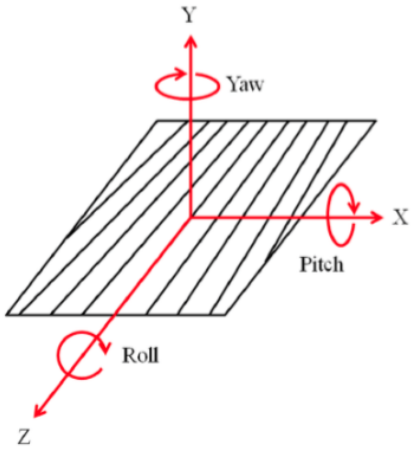

Fig. 4.—: Definitions for the six degrees of freedom with respect to a grating. (Allured et al. 2015).

Table 1:: Analytical Alignment Tolerances from Allured & McEntaffer 2013

Degree of Freedom	Tolerance	Limiting Effect
Yaw	±7.9 arcsec	Effective area
Pitch	±4.3 arcsec	Effective area
Roll	±21.6 arcsec	Spectral resolution
$\hat{x}$	±317 μm	Effective area
$\hat{y}$	±170 μm	Effective area
$\hat{z}$	±1.51 mm	Spectral resolution

The primary goal of the alignment performance tests in **Section 3.3** was constraining the angular degrees of freedom. Thus, there was more concern about the yaw, pitch, and roll misalignments than the translational misalignments. In order to prove the feasibility of using our alignment method for future use, the degree of grating-to-grating angular misalignment occurring within the module must stay within the analytical tolerances in **Table 1**.

3. Procedure

3.1. Module Design

The off-plane grating module used in the investigation was composed of a titanium housing with built-in flexures and bonded carbon-fiber inserts on both sides (Allured et al.

2015). The titanium housing was used to ensure both mass and stiffness, and the carbon-fiber inserts were used to act as an interface between the housing and gratings in order to eliminate excessive thermal issues. The flexures, which were machined to hold each grating in place, were bonded to the grating substrate before the alignment process. A total of fifteen 100-by-75 mm format, 0.5 mm thick glass plate gratings were aligned and bonded within the module. A comparison between the mechanical design of the module and the final product is shown in **Figures (a) and (b)**.

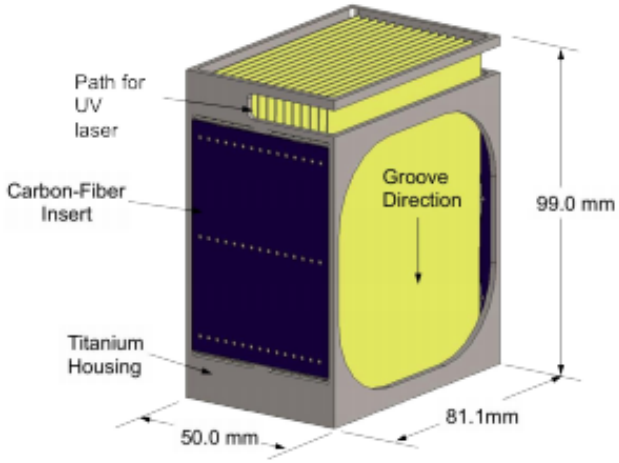

(a) Mechanical design of grating module. (Allured et al. 2015)

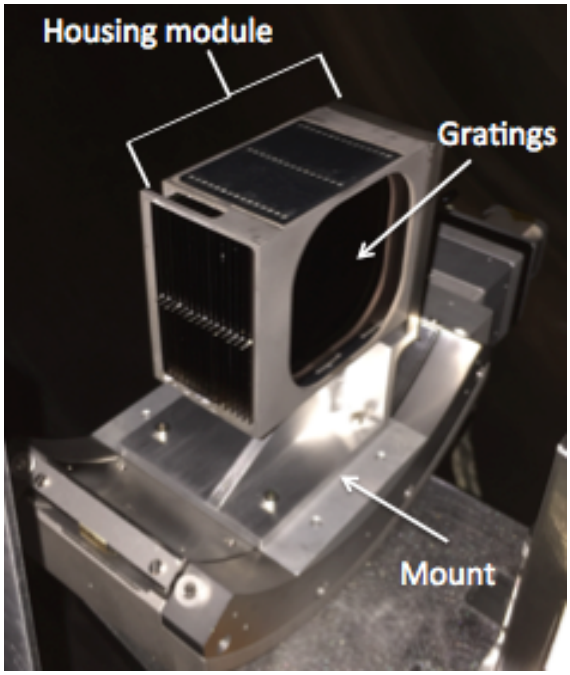

(b) Aligned grating module.

3.2. Grating Alignment

The entire setup was aligned in the configuration shown in **Figure 5** using a collimated infrared laser beam (Allured et al. 2015). The first grating plate was then installed in the module and mechanically constrained on the mount. A Shack-Hartmann wavefront sensor metrology system was used to monitor and measure the pitch, roll, and figure of the grating during alignment, and a collimated UV diffraction laser was used to monitor the grating's yaw. The UV laser was also used to produce both a specularly reflected beam and a Littrow back-diffracted beam, which were both monitored and centered using Mightex cameras.

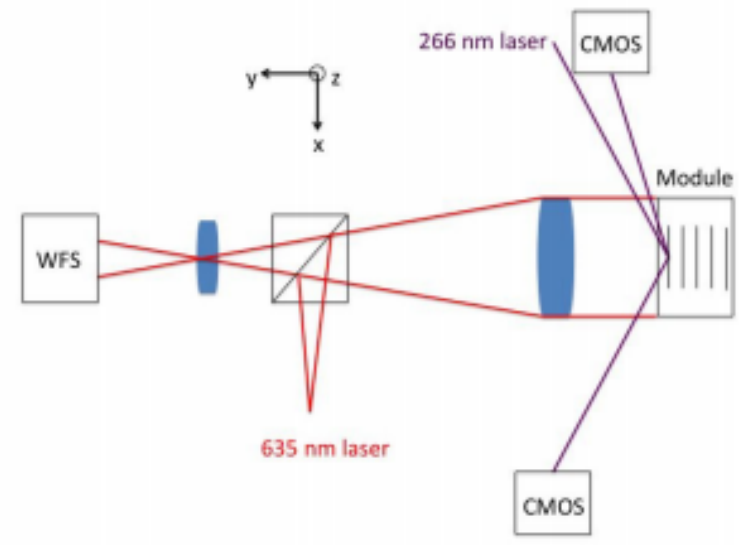

Fig. 5.—: Conceptual diagram of the alignment methodology. WFS refers to the wavefront sensor, and CMOS refers to cameras put in place to monitor the zero order and sixth order diffraction spots. (Allured et al. 2015).

A hexapod, a device enabling movement in any of the six degrees of freedom, was used for the fine alignment of each grating. Using the hexapod, the pitch and roll of the grating were manipulated until the angles were zeroed with respect to the module, and yaw was adjusted until the diffracted beam was in complete alignment with the grating. The grating was then bonded into place, and the procedure was repeated for the next grating.

An indexing procedure was implemented in order to ensure that the next grating was inserted into the same location as the previous one relative to the WFS. This involved indexing the module position for the installation of each grating, and fixing an optical reference flat to the module support plate to ensure that the module's pitch and roll angles did not change during indexing.

The end result of this process was fifteen 100-by-75 mm format, 0.5 mm thick glass plate gratings with proper relative alignment to one another within the module for a converging X-ray beam. The gratings were bonded to the carbon-fiber inserts using fused silica rods. The final setup at the Smithsonian Astrophysical Observatory is shown in both **Figure 6** and **Figure 7**.

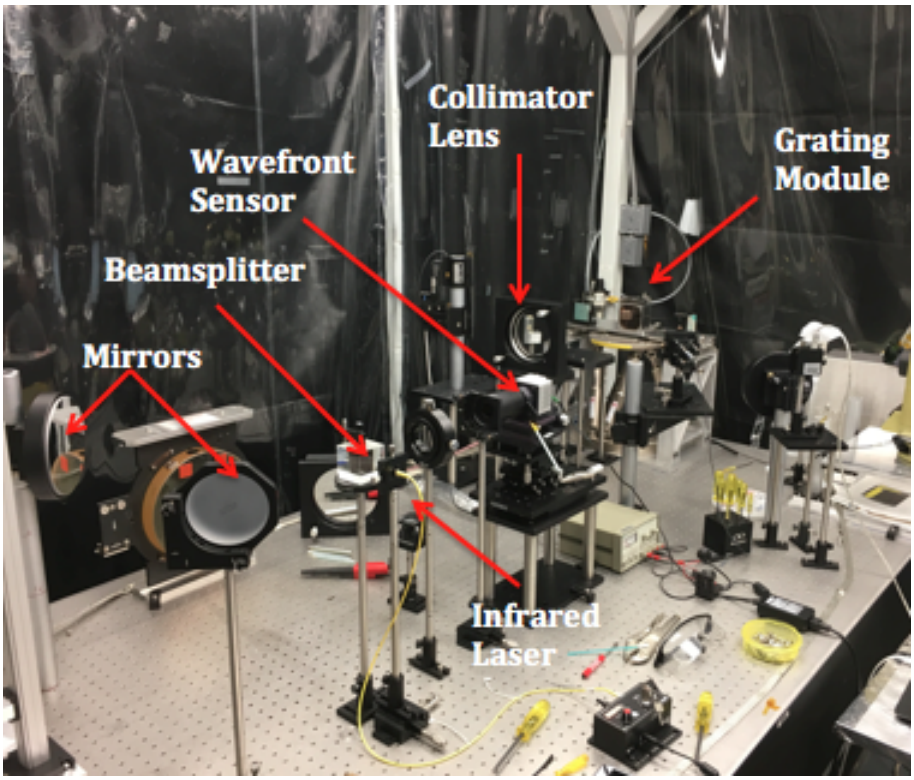

Fig. 6.—: Alignment setup at SAO.

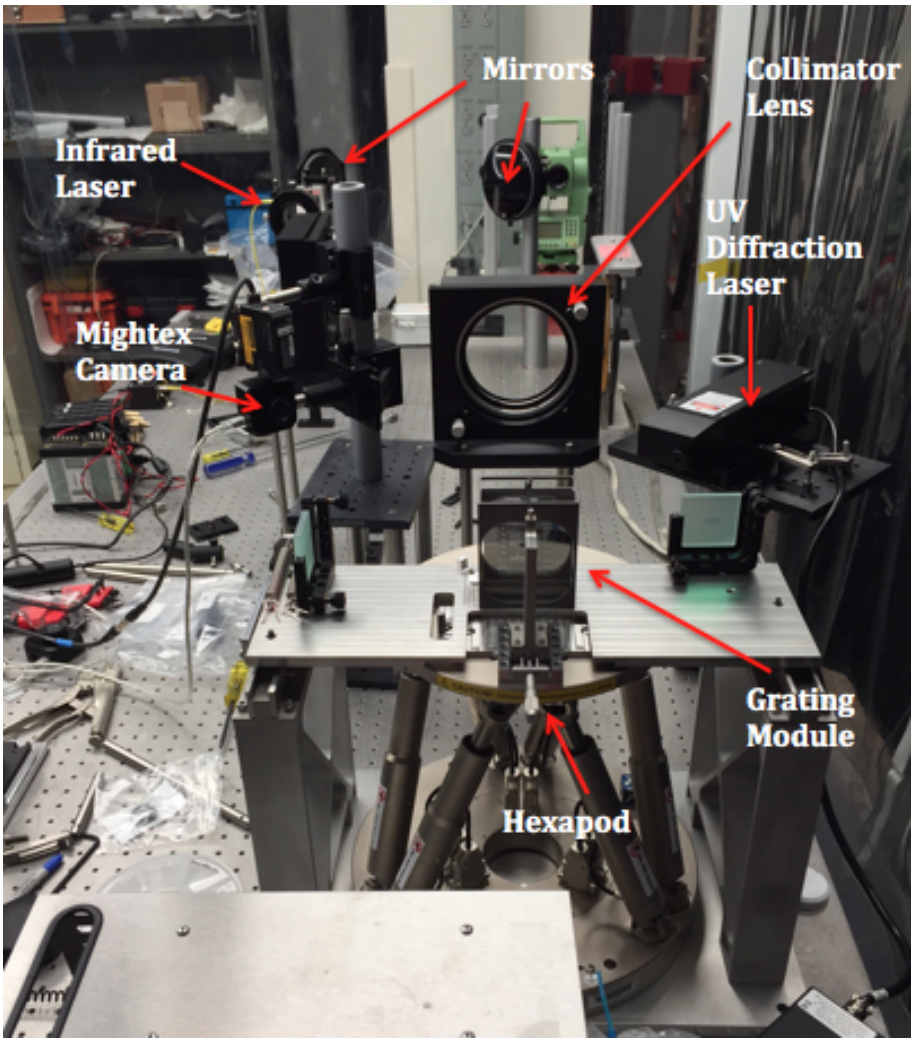

Fig. 7.—: Alignment setup from point-of-view of grating module.

3.3. Alignment Performance Test Overview

A series of alignment performance tests in the X-ray were done throughout the week of October 3rd, 2016 at the NASA Marshall Space Flight Center. A brief breakdown of this procedure is as follows: **1)** CCD camera, SPO module, and grating module were installed and aligned in a vacuum chamber (proper setup and alignment shown in **Figures 8 and 9**); **2)** to verify the alignment technique, pre-test measurements of grating-to-grating alignment were taken by imaging the location of the zero order and sixth order diffraction spots; **3)** vibrational tests were administered to ensure that the module can survive orbital ascent; **4)** a thermal test was administered to ensure that the module could experience large thermal gradients; **5)** post-environmental measurements of grating-to-grating alignment were taken.

The alignment setup in the chamber consisted of the off-plane reflection grating module, a silicon pore optic (SPO) module (**Figure (a)**), and a CCD camera. The SPO, which consisted of more than 40 layers of silicon wafers, was used as a grazing-incidence mirror (Smith et al. 2016). The grating module was aligned to the SPO focus so that the X-ray beam would be diffracted along the narrow point-spread-function direction as shown in **Figure (b)** below, thus optimizing spectral resolving power.

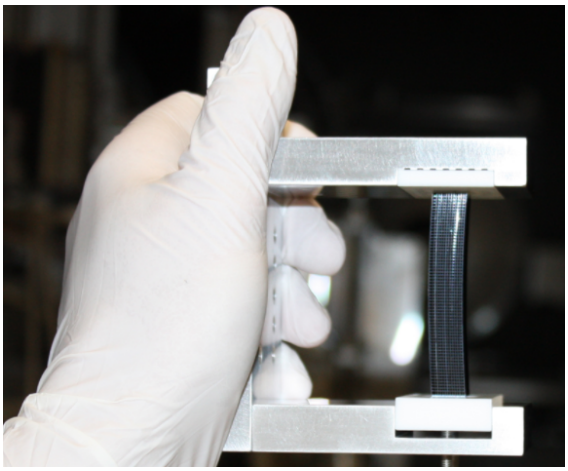

(a) Silicon Pore Optic module (Marlowe et al. 2015)

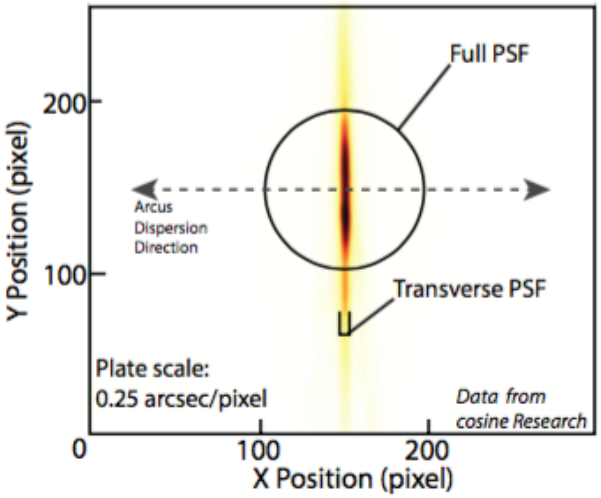

(b) Ideal SPO Point Spread Function (Smith et al. 2016)

Pre-test measurements of the grating-to-grating alignment were taken in order to verify that our alignment technique was feasible. Post-test measurements of the alignment were taken to ensure that the mechanical and structural design of the module was sound. The CCD camera aligned at the focal plane was used to take images of the zero order (reflected) spot and the highest diffraction order (sixth) spot.

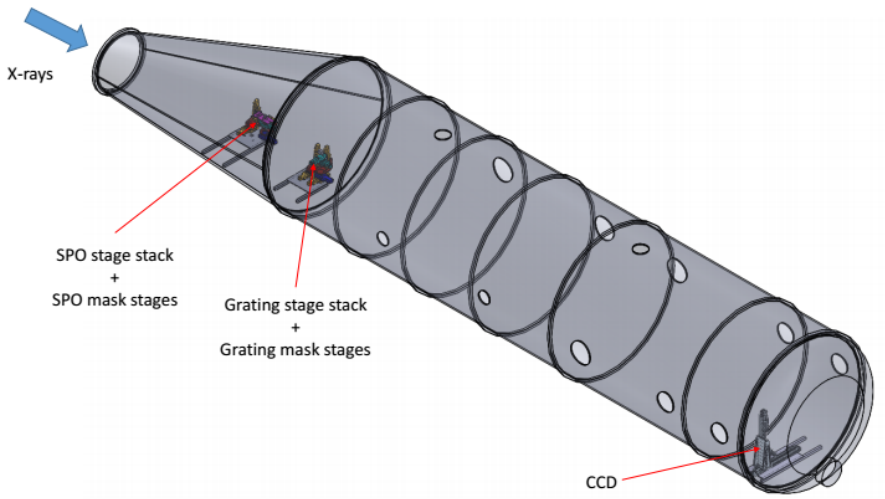

Fig. 8.—: Overview of test set-up. An X-ray point source was leveled outside of the chamber and aligned with the off-plane grating module. The SPO module was mounted and aligned behind the OPG module in order to achieve the diffraction geometry described in **Section 2**. The CCD was aligned at the focal plane. (Diagram created by R. McEntaffer).

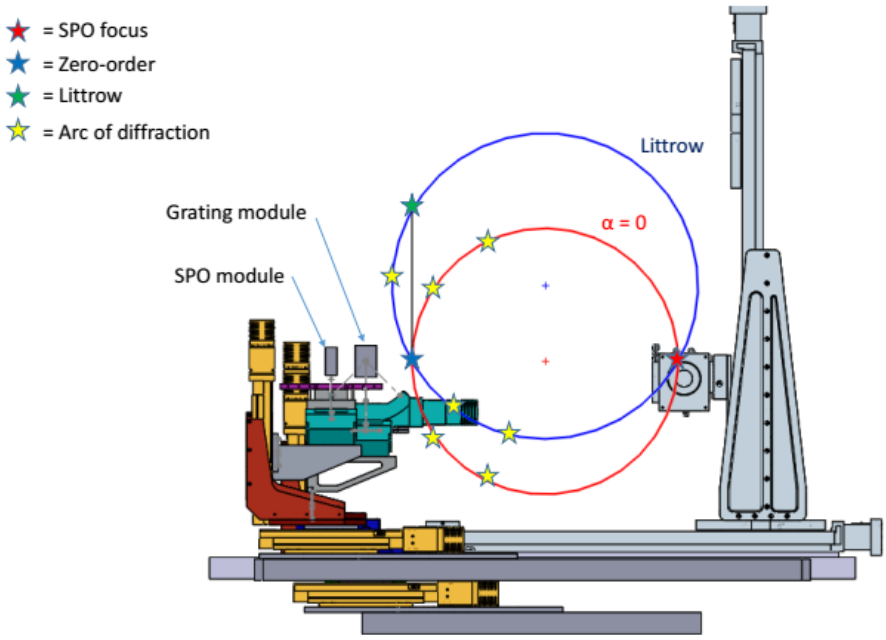

Fig. 9.—: Minimized view of the OPG-SPO-CCD alignment down the beam/optical axis. The test was set up so that the detector stage position would not have to be changed. Given that constraint, the optics and gratings were placed so that the telescope focus (red star) and the diffraction arc in the Littrow configuration (blue circle) could still be sampled. (Diagram created by R. McEntaffer)

4. Data Reduction

4.1. Photon Count Procedure

With raw images of both the zero order reflection and sixth order diffraction from the CCD camera for each grating, the next step was employing image correction in order to separate the pixels containing photon events from the background pixels. This is a complicated process, as one must not only be wary of false positives (pixels barely clearing threshold) and hot pixels/cosmic rays (outlier pixels much higher than regular photons), but also be considerate of split events, photons that take up more than one pixel. Simply binning each pixel that clears a certain threshold and counting it as a single event left open the possibility of double-counting photons that cover multiple pixels.

The first step was separating the photons from the background by subtracting the raw science image's respective dark image from it. To perform the dark image subtraction, a pixel-by-pixel median of all of the dark image's frames was taken, resulting in a CCD-sized master dark $\mathbf{M_{dark}}$ array where each pixel represented the median response of that particular pixel in all of the dark frames. The median is useful because it is insensitive to the outliers due to hot pixels or cosmic rays - if a pixel is too high, it gets cut rather than pulling the average higher.

The next step was "grading" the photon events, which involved defining a threshold value that background pixels would fall below and photon events would clear. The dark frames were used once again to construct a variance dark $\sigma_{\mathbf{dark}}$. A pixel-by-pixel standard deviation of the dark frames was taken, ending up with a CCD-sized array where each pixel represented that pixel's sigma. A grade threshold of $\mathbf{10}\sigma$ was ultimately chosen and used to determine which pixels were above this variance frame. In summation, the identification of possible photon events was defined using the following expression:

$$\text{Photon Events} = [\text{Frame - } M_{dark} \text{ - } \sigma_{dark} * 10\sigma] > 0 \tag{1}$$

This subtraction returned an analog-to-digital conversion (ADC) "grade" for each pixel in the science image frame. The pixels meeting the stated criteria were considered possible photon events, and the pixels with values less than 0 were deemed background noise. However, this subtraction did not account for split events or hot pixels that had spuriously higher grades than photons. To handle split events, an algorithm was coded to create an array of 3x3 islands around every pixel. This allowed for correctly counting which pixels in the island satisfied the event criteria. For hot pixels, plotting the photon events as a function of ADC value showed an abundance of outliers beyond a value of 300 ADC. As a result, an

upper limit of 300 ADC was set to ignore these outliers. **Figure 10** shows a histogram of the number of photon events identified using a 5σ threshold for a single grating, while **Figure 11** shows a histogram of events identified using a 10σ threshold for all of the gratings combined.

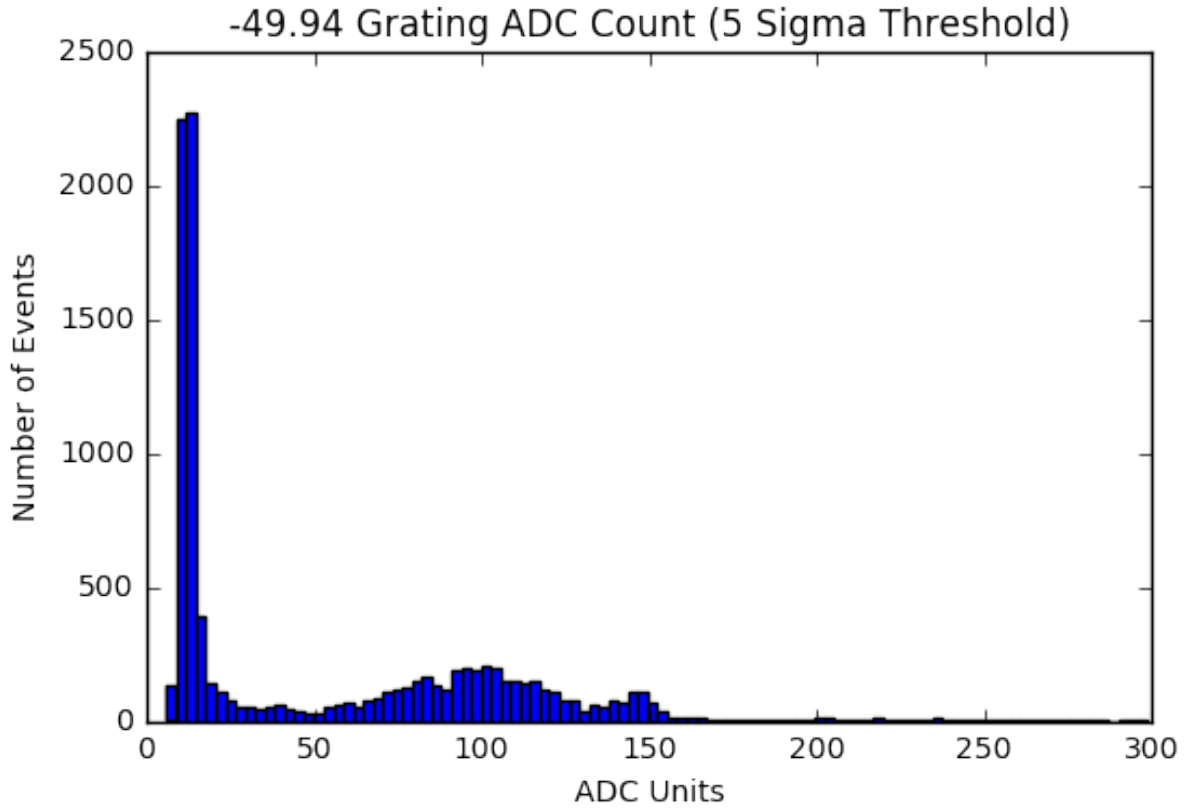

Fig. 10.—: ADC count histogram for a single grating, using a 5σ grade threshold above the background. This grade threshold resulted in too many false positives, so a higher value was needed.

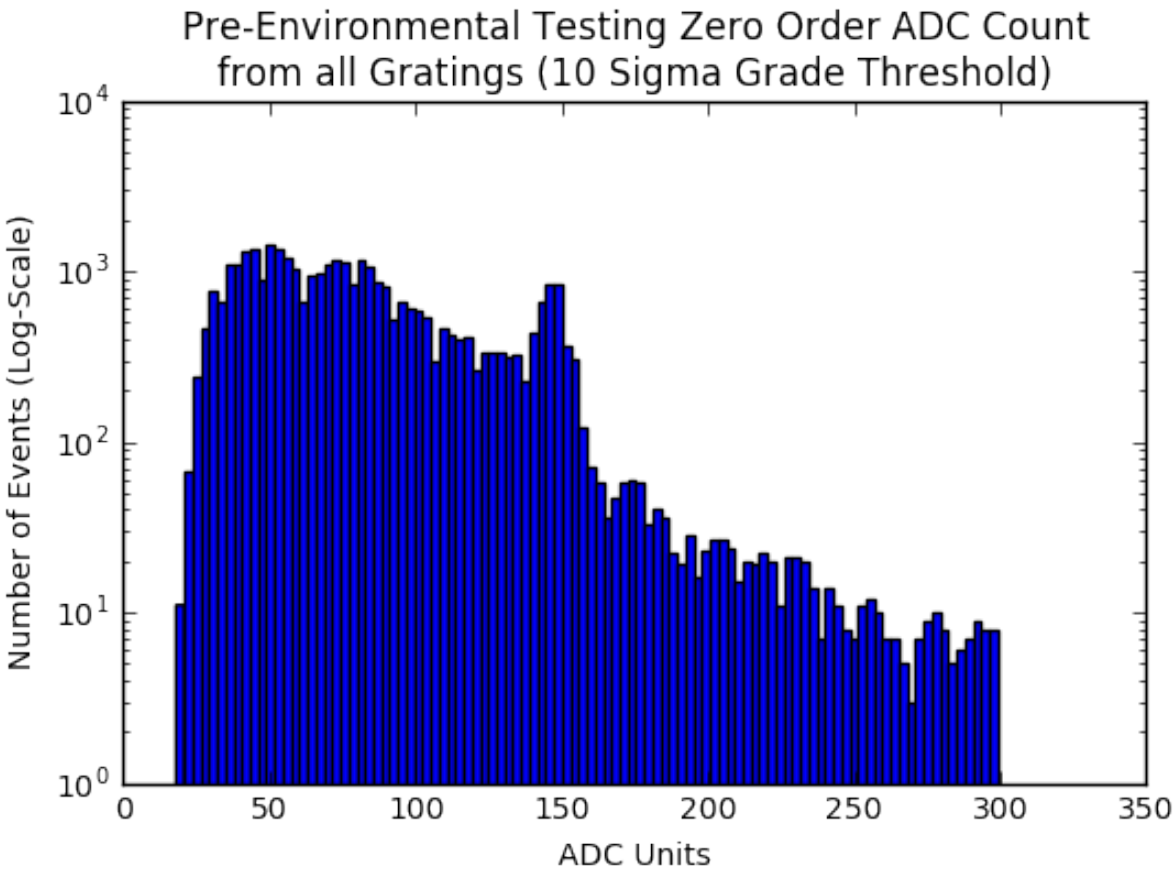

Fig. 11.—: Combined ADC count histogram for all gratings, using a 10σ grade threshold above the background. This grade threshold was high enough to eliminate the false positives.

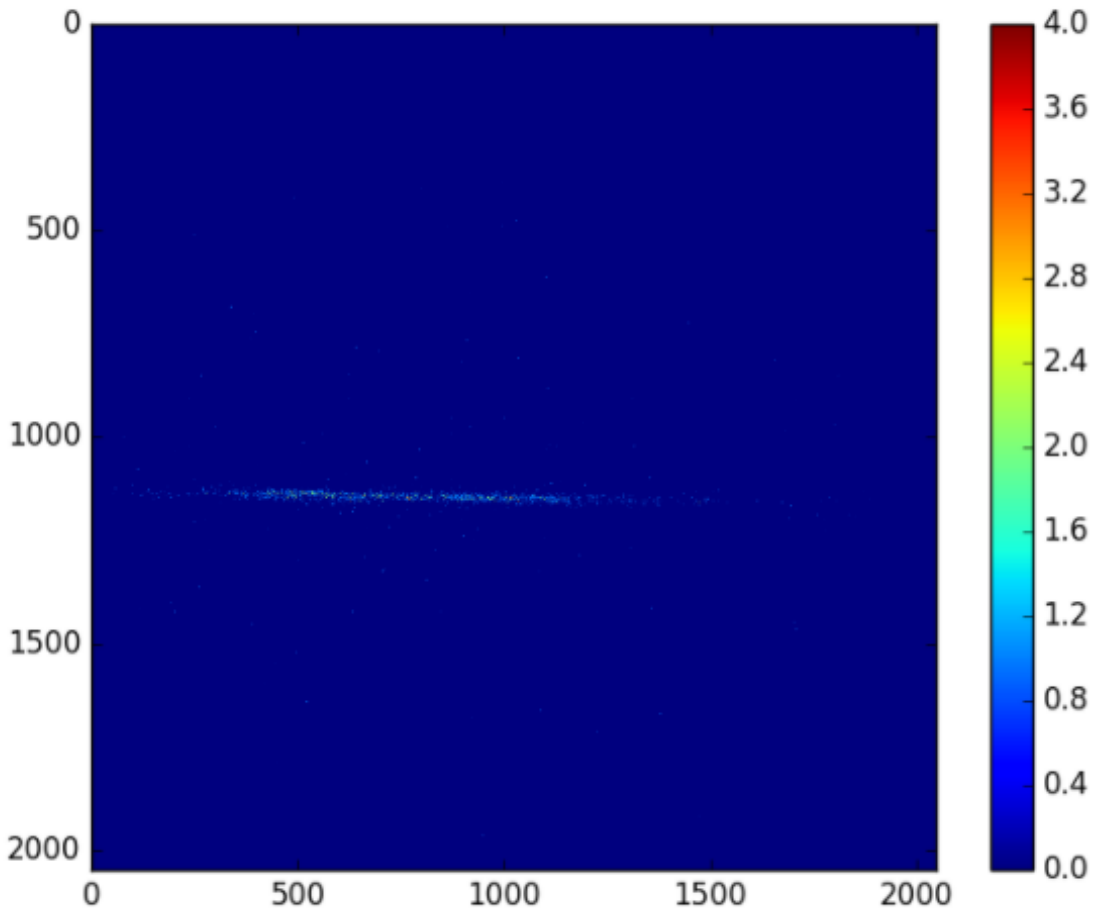

Fig. 12.—: Binary image of pre-environmental testing zero order line spread functions for a single grating (10 Sigma Grade Threshold).

A binary image where every detected event was given a value of 1 and every other pixel was given a value of 0 is shown in **Figure 12** for the zero order reflection of a single grating. This data reduction procedure was run for each grating's raw zero order reflection image and sixth order diffraction image. From this process, we were able to extract the x-axis (dispersion distance) position, y-axis (cross-dispersion distance) position, and grade of every photon in every image for each grating. **Figures 13-16** in **Section 4.2** show the measurements for zero and sixth orders both before and after environmental testing, with color-coded photons from each grating.

4.2. Photon Count Results

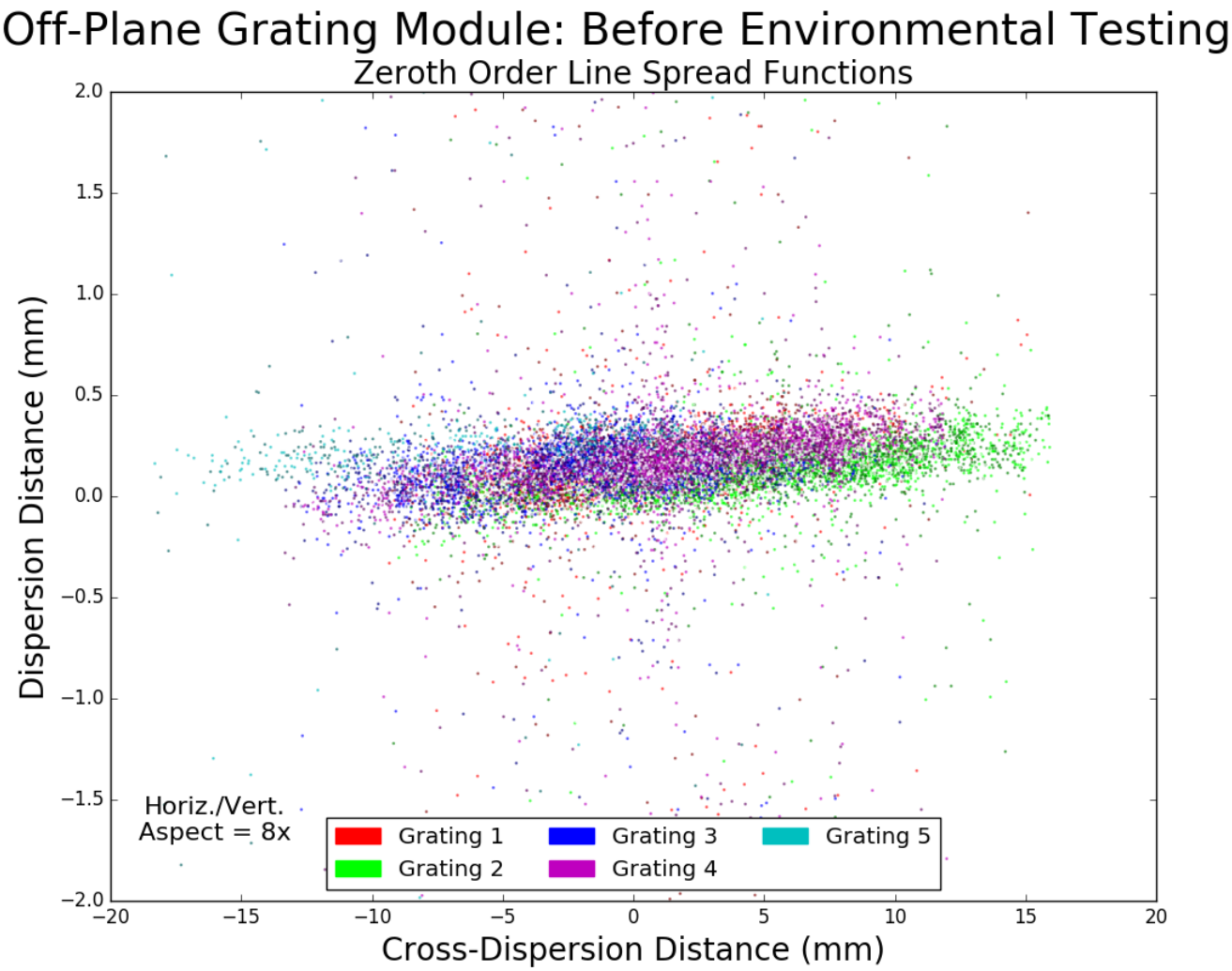

Fig. 13.—: Pre-environmental testing zero order line spread functions for each grating in the off-plane grating module. The photons from each grating (color-coded) are graphed on top of one another to show the degree of misalignment that occurred.

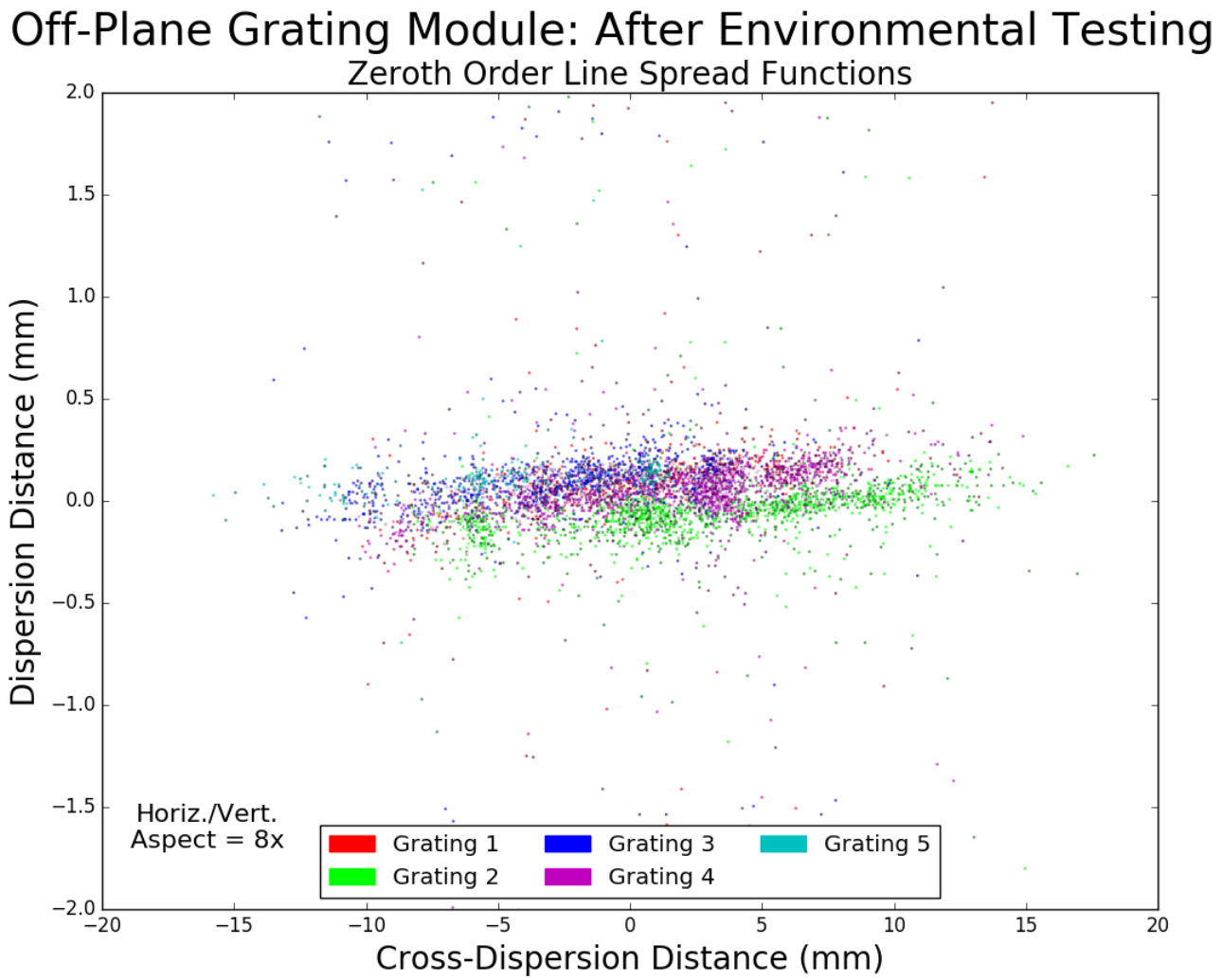

Fig. 14.—: Post-environmental testing zero order line spread functions for each grating in the off-plane grating module.

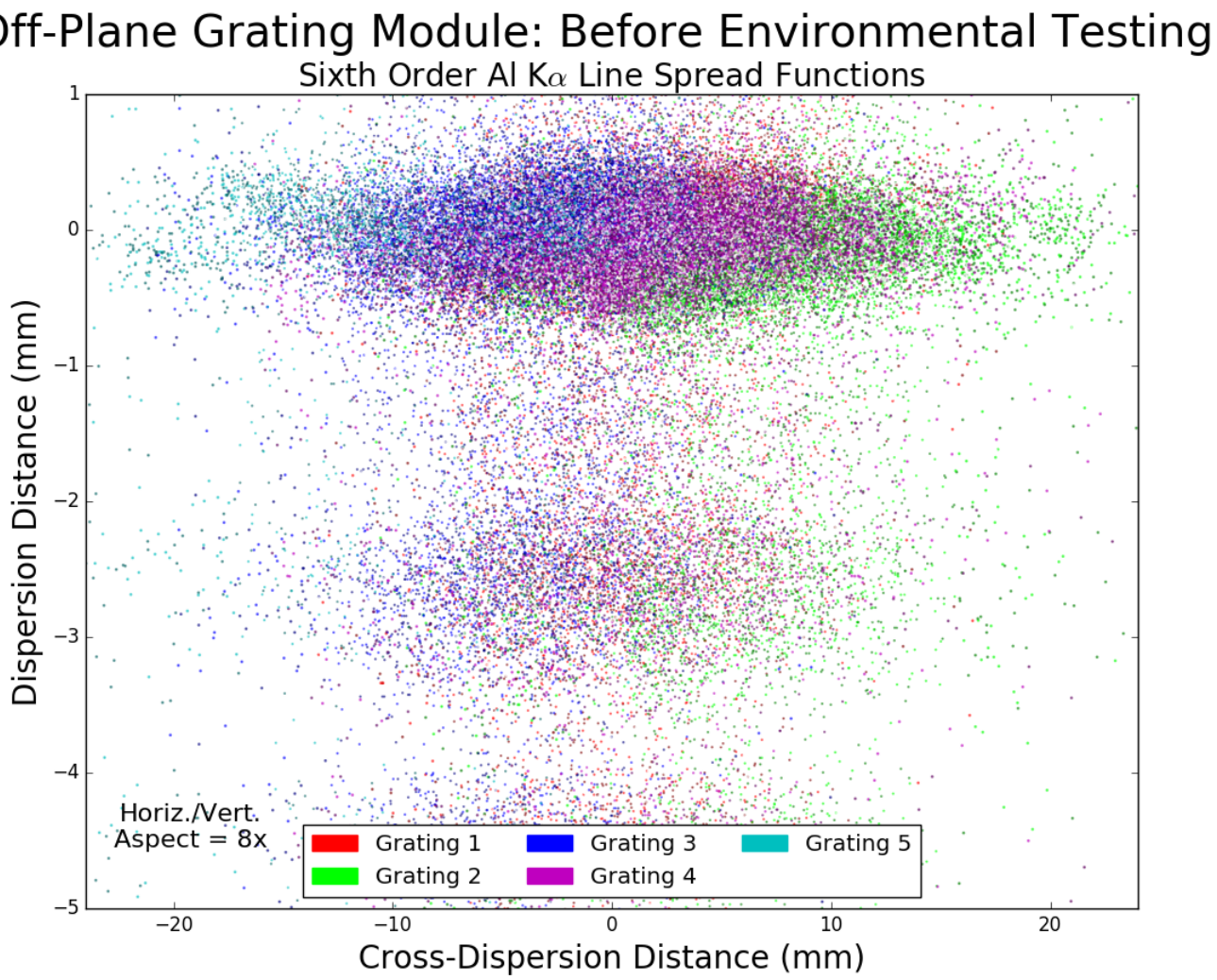

Fig. 15.—: Pre-environmental testing sixth order line spread functions for each grating in the off-plane grating module.

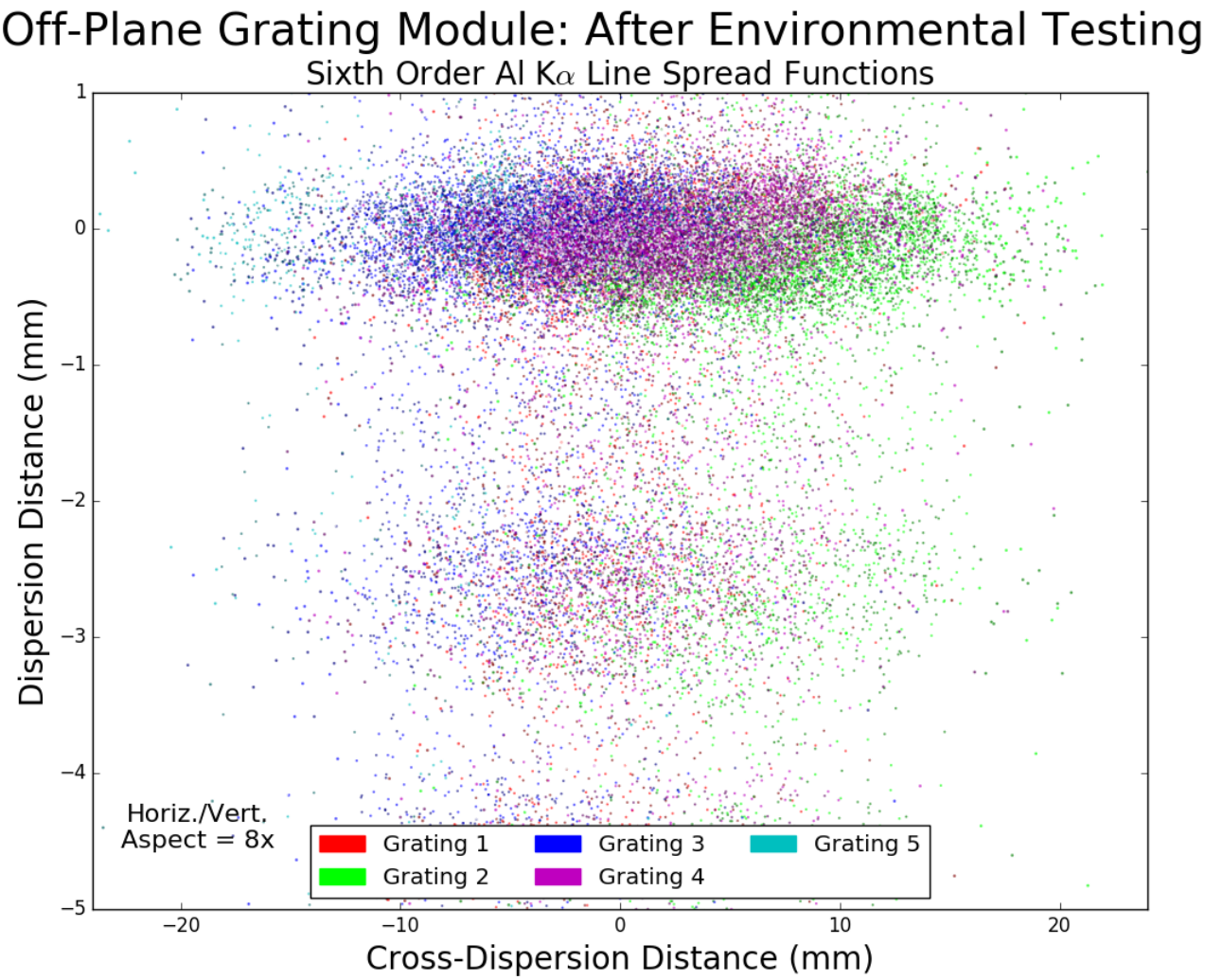

Fig. 16.—: Post-environmental testing sixth order line spread functions for each grating in the off-plane grating module.

5. Grating-to-Grating Angular Misalignments

5.1. Raytracing Sensitivity Analysis

The data collected from the photon analysis gave the parameters necessary to calculate shifts between gratings. However, a raytracing sensitivity analysis was required in order to calculate the actual angular misalignments. Alignment sensitivities for the off-plane grating module were determined via geometric raytracing codes developed at SAO by R. Allured. Similar to the tests at MSFC, this analysis was performed assuming the nominal X-ray test geometry. A diverging bundle of rays from an X-ray point source was fed into the SPO module, diffracted from the OPG module, and finally traced to the focal plane. The centroid coordinates of the ray bundle were subsequently recorded. Next, for a given degree of freedom, a misalignment was introduced to the OPG module and the shift in the centroid of the ray bundle was calculated.

The linear relationship of centroid shift versus misalignment (shown in **Figure 17**) was derived using the resultant centroid positions, allowing for the calculation of the sensitivities for both zero order and for sixth order Al K line spread functions as shown in **Tables 2 and 3**. Centroid shifts were converted to arcseconds of error at the focal plane, angular sensitivities were expressed in arcseconds per arcsecond, and translational sensitivities were expressed in arcseconds per millimeter.

Table 2:: Zero Order Linear Sensitivities for Grating Module

Direction	Yaw (arcsec/arcsec)	Pitch (arcsec/arcsec)	Roll (arcsec/mm)
Cross-Dispersion	Negligible	1.98	Negligible
Dispersion	Negligible	Negligible	0.052

Table 3:: Sixth Order Linear Sensitivities for Grating Module

Direction	Yaw (arcsec/arcsec)	Pitch (arcsec/arcsec)	Roll (arcsec/mm)
Cross-Dispersion	1.23	2	0.0659
Dispersion	Negligible	Negligible	0.050

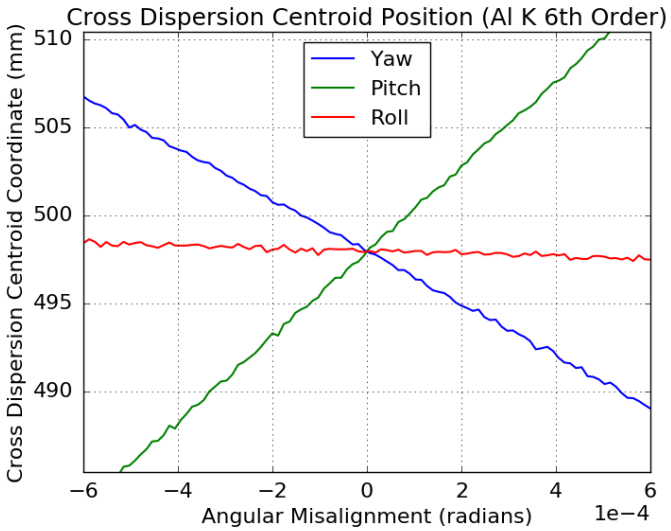

Fig. 17.—: Plot showing how the cross-dispersion centroid coordinate changed with misalignment in the yaw, pitch, and roll angles.

5.2. Measured Misalignments

In order to measure the misalignment between two gratings, the centroid pixel from one grating was found and compared to the relative centroid pixel in the second grating. The global position of the CCD had to be accounted for in this computation, as it was continually shifting between positions. The horizontal position of the CCD did not move, but the vertical position did for each grating. As a result, the CCD origins were different for various gratings and had to be taken into account in order to assess alignment.

After finding the zero order and sixth order centroids for both the pre-test and post-test line spread functions, the position values were put in the same referenced global coordinate system. Only angular misalignment was assumed, and was calculated from the linear sensitivities from the zero order pitch (cross-dispersion) centroids, zero order roll (dispersion) centroids, and sixth order yaw (cross-dispersion) centroids. Finally, the standard deviation of the five measured misalignments were taken. The final pre-test and post-test misalignment measurements are shown in **Table 4**.

Table 4:: Pre-Environmental and Post-Environmental Misalignment Standard Deviations

Test	Pitch (arcsec)	Roll (arcsec)	Yaw (arcsec)
Pre-Test	34.2 (±0.2)	25.4 (±0.3)	36.7 (±0.1)
Post-Test	25.0 (±0.3)	17.1 (±0.2)	59.4 (±0.5)

6. Discussion and Future Directions

Comparing the **Table 4** misalignment measurements to the analytical tolerances in **Table 1**, we were unable to effectively constrain the angular degrees of freedom with our current alignment technique. However, considering that this experiment was the first test for the particular alignment technique used, this investigation merely serves to identify some of the problems we would need to study in order to move forward. Though the measured misalignments were outside of the analytical tolerances derived, the fact that we were within a factor of 2-3 of our tolerances on the first try is a very encouraging result. From this investigation, we can take away that this technique could potentially work but refinement is necessary.

In terms of future directions, the next step would be identifying and understanding the cause of the excessive misalignment. Since there was a disagreement between the analytical tolerances and measured misalignments, there is most likely is a systematic error in either the alignment technique or in the data reduction process. One short-term goal would be fleshing out this possible error source in order to better understand how to improve upon the alignment technique. If there is a systematic error, that indicates the possibility that the gratings moved slightly during the environmental tests, most likely the vibrational test. If this is the case, an investigation of epoxy bonding may be necessary to understand the full impact of the environmental effects.

This grating system was originally intended for the Arcus X-ray grating spectrometer, a medium Explorer-class mission proposal that, if approved by NASA, would be deployed as a free-flying satellite (Smith et al. 2016). The planned spectrometer would ideally enable high-resolution spectroscopy and achieve higher spectral resolution than the *Chandra* and the *XMM-Newton*. The spectrometer was originally designed to utilize off-plane gratings, but due to unforeseen circumstances, the team has switched to using a critical-angle transmission grating system. Despite the switch, this investigation was still useful in terms of showing that, with some refinements, our alignment technique for an off-plane grating system can potentially be used for future x-ray spectrometers.

7. Conclusion

We have presented an analysis of one alignment technique used for an off-plane reflection grating system. An off-plane grating module was successfully designed and assembled in a flight-like mount, and set up in an MSFC facility chamber with an SPO module and CCD camera to produce nominal diffraction geometry in the X-ray. The module's grating-to-grating alignment performance was effectively tested both before and after implementing vibrational and thermal tests. Data reduction of the raw images taken by the CCD yielded the desired number and positions of photon events (line spread functions) for both the zero order and sixth order diffraction spots. Finally, the measured grating-to-grating angular misalignments were successfully calculated after deriving the cross-dispersion - angular misalignment relationship in a raytracing sensitivity analysis. The yielded misalignments were outside but not too far off of the analytical alignment tolerances derived in *Allured & McEntaffer 2013*, which was encouraging for the first attempt using this alignment technique. Further refinement of the technique will be required to truly gauge the technique's potential.

8. Acknowledgments

I would like to thank my advisors Randall Smith, Casey DeRoo, and Ryan Allured for this research opportunity, as well as their guidance and assistance with this project.

REFERENCES

Allured, R. et al. 2015. "Optical and X-ray Alignment Approaches for Off-Plane Reflection Gratings." *Proceedings of the SPIE*, Volume 9603, id. 960315.

Allured, R. and McEntaffer, R. 2013. "Analytical Alignment Tolerances for Off-Plane Reflection Grating Spectroscopy." *Exp Astron*, 36:661-677.

DeRoo, C. et al. 2016. "Line spread functions of blazed off-plane gratings operated in the Littrow mounting." *Journal of Astronomical Telescopes, Instruments, and Systems*, 2(2), 025001.

Lumb, D. et al. 2012. "XMM-Newton (X-Ray Multi-Mirror Mission) Observatory." *eprint arXiv:1202.1651.*

Marlowe, H. et al. 2015. "Performance Testing of an Off-Plane Reflection Grating and Silicon Pore Optic Spectrograph at PANTER." *Journal of Astronomical Telescopes, Instruments, and Systems*, 1(4): 045004.

McEntaffer, R. et al. 2013. "First results from a next-generation off-plane X-ray diffraction grating." *Experimental Astronomy*, 36(1): 389-405.

Simionescu, A. et al 2011. "Baryons at the Edge of the X-ray-Brightest Galaxy Cluster." *Science*, 331(6024):1576.

Smith, R. et al 2016. "Arcus: The X-ray Grating Spectrometer Explorer." *Submitted to Proceedings of the SPIE.*

Tananbaum, H. et al. 2014. "Highlights and Discoveries from the Chandra X-ray Observatory." *Reports on Progress in Physics*, 77(6): 066902.

Weisskopf, M. et al. 2002. "An Overview of the Performance and Scientific Results from the *Chandra X-Ray Observatory.*" *Publications of the Astronomical Society of the Pacific*, 114:1-24.